Onset of non-linear IV transport with magnetic order in a Mott insulator

Tanya Berry[†,‡,*], Nicodemos Varnava[§], Dominic Ryan[¶], Veronica Stewart[†,‡], Riho Rästa[#], Ivo Heinmaa[#], Nitesh Kumar[††], Walter Schnelle[††], Rishi Bhandia[‡], Christopher Pasco[1,2], N. P. Armitage[‡], Raivo Stern[#], Claudia Felser[††], David Vanderbilt[§], Tyrel M. McQueen[†,‡,‡‡]

† Department of Chemistry, The Johns Hopkins University, Baltimore, Maryland 21218, USA
‡ Institute for Quantum Matter, William H. Miller III Department of Physics and Astronomy, The Johns Hopkins University, Baltimore, Maryland 21218, USA
§ Department of Physics & Astronomy, Rutgers University, Piscataway, NJ 08854, USA
¶ Physics Department and Centre for the Physics of Materials, McGill University, 3600 University Street, Montreal, Quebec, H3A 2T8, Canada
# National Institute of Chemical Physics and Biophysics, Akadeemia tee 23, 12618 Tallinn, Estonia
†† Max-Planck-Institute for Chemical Physics of Solids, D-01187 Dresden, Germany
‡‡ Department of Materials Science and Engineering, The Johns Hopkins University, Baltimore, Maryland 21218, USA

*Corresponding author email: tberry@ucdavis.edu

Abstract:

Nonlinear electrical transport phenomena underlie a plethora of electronic components and devices, and are often used to identify and probe novel ground states in quantum materials. Herein we report a non-linear voltage and current relationship in the layered magnetic semiconductor $EuMn_2P_2$, which develops below its magnetic ordering temperature at $T_N \approx 17$K. Such behavior is known for materials that have charge density wave order, are proximal to a metal-insulator transition, or have complementary p- and n-type doping. However, none of the preceding apply to $EuMn_2P_2$, which exhibits a transition from linear to non-linear voltage-current behavior associated with Eu^{2+} magnetic ordering. The non-linearity is nearly magnetic field independent, and likely arises from a change in band level alignment between $EuMn_2P_2$ and the metallic contacts due to exchange splitting of antiferromagnetic $(Mn_2P_2)^{2-}$ bands due to Eu^{2+} antiferromagnetic order. This discovery demonstrates a novel approach to building electronic devices from antiferromagnetic insulators and to probing quantum magnetic states of matter.

Strongly correlated materials with large electron-electron interactions display a variety of exotic electrical and magnetic properties as seen in Kondo insulators,[1-3] spin and charge density wave systems,[4,5] hydrodynamic materials,[6,7] superconductivity,[8,9] and beyond.[10-14] The precise electronic/magnetic ground state is determined by a subtle interplay between electron-nuclear and electron-electron interactions that is set by the local atomic bonding between atoms. When a material's structure has two distinct magnetic subunits, then the separation of energy scales within and between subunits can give rise to distinct behaviors that would not arise with a single homogeneous magnetic lattice. For example, the coexistence of magnetism and superconductivity in $Ho_2Ni_2B_2C$ arises due to localized 4f magnetism in HoC layers coupled to superconductivity in Ni_2B_2 layers.[15] The interactions between subunits can be more directly coupled, and depending on the balance of charge and spin interactions, drive subunits to different ground states. For example, the metal $EuFe_2As_2$, which crystallizes in the $ThCr_2Si_2$ crystal structure, exhibits separate magnetic ordering transitions for the anionic $(Fe_2As_2)^{2-}$ framework and cationic Eu^{2+} layers at ambient pressure.[16] Under chemical or epitaxial pressure, there is partial additional charge transfer to the

$(Fe_2As_2)^{2-}$ framework, which results in superconductivity, with residual weak magnetism in the Eu layers.[16]

In this work we investigate $EuMn_2P_2$, which crystallizes in a trigonal $CaAl_2Si_2$-type structure (space group *P*3-m1). $EuMn_2P_2$, has previously been reported as having a magnetic Eu^{2+} cationic layers separated by non-magnetic $(Mn_2P_2)^{2-}$ polyanionic subunits that are reported to be non-magnetic.[17] The property of Mn being non-magnetic in $EuMn_2P_2$ is puzzling since isoelectronic $EuMn_2As_2$ and $EuMn_2Sb_2$ have Mn magnetic order.[18-20] Here we report discovery of hidden Mn magnetic ordering and the appearance of spontaneous non-linear voltage-current transport when the cationic Eu^{2+} sublattice magnetically orders. This non-linearity is driven due to the exchange splitting of states derived from the antiferromagnetic $(Mn_2P_2)^{2-}$ layers upon Eu^{2+} magnetic order at $T_N \approx 17$K.

Our findings are summarized in Fig. 1 (see SI for detailed methods). At $T = 20$ K, Fig. 1A, the *IV* curve is linear, as expected for a semiconductor with ohmic contacts (Pearson $R^2 = 0.99961$). A small non-linearity is observable at T = 15 K, Fig. 1B ($R^2 = 0.99942$), which then becomes more pronounced at lower temperatures, Fig. 1C,D ($R^2 = 0.99559$ and 0.97963). We can quantitatively model this non-linear behavior using a two-channel model consisting of a resistor in parallel with a pair of opposing Schottky diodes, representing contacts, with an included series resistance, Fig. 1D inset. Assuming the two diodes have the same characteristic parameters, there are four refinable parameters: the normal channel resistance (R_p), the diode saturation current (I_s), carrier-weighted threshold voltage (nVt), and diode series resistance (R_s); values are tabulated in Table-SI. While this model provides a suitable description of the behavior, it does not identify its microscopic origin. Indeed, the resultant parameters indicate the behavior is not of the simple Schottky variety:[21] nVt is the thermal voltage ($= k_BT/e \sim 0.00028$ V @ 3 K) in the Schottky model times a number of order unity – but nVt is ~ 1.5 V, which would make the "number of order unity" = ~5000, unphysically large. One common extrinsic origin for non-linearity is sample self-heating. Two considerations exclude such joule heating as an origin of the observed non-linearity: (i) R_p increases by a factor of more than 10^5 from $T = 10$ K to $T = 2$ K, whereas it would be expected to remain ~constant if heating dominates (R_s similarly increases by a factor of ~6); (ii) the total power dissipated (including contacts) at $T = 2$ K is $0.3\mu A \cdot 10V = 3\ \mu W$, much less than the ~10 mW of cooling power of the stage at base temperature. Other common intrinsic origins are also excluded: the compound is valence precise and thus not unstable to charge density wave order; and linearity at $T \geq 20$ K excludes a p-n junction from inadvertent chemical doping.

Instead, it appears that this behavior coincides with the formation of europium magnetic order. The magnetic hyperfine field (B_{hf}), determined by ^{151}Eu Mössbauer spectroscopy Fig. S1,S2 and Fig.1E, shows the appearance of magnetic order at $T_N = 17$ K. Magnetic order on Eu is further confirmed by magnetization (Fig. S3,S4,S5) and zero field NMR measurements (Fig. S6, Table SII). The appearance of magnetic order correlates with the non-linear transport behavior: if we use the fraction of current flowing through the diodes in our two channel equivalent circuit as an effective order parameter, it shows an initial turn-on at $T_N \sim 17$ K, with a steep rise around $T \sim 13$ K. This suggests that the Eu magnetic order is driving the observed non-linearity in electrical transport. The mechanism, however, is cannot be direct band shifts due to an internal magnetic field: there is no qualitative change in the *IV* behavior up to a magnetic field of 9 T when the field is applied perpendicular to the current direction, Fig. 1F, even though this field is sufficient to fully polarize the Eu moments (vida infra). A similar independence is also found

as the angle of the applied magnetic field is rotated to be parallel to the current direction (Fig. S7,S8, Table SIII). This near field independence instead suggests the behavior is due to a more fundamental change in electronic structure with the appearance of Eu magnetic order.

We use density functional theory (DFT) within GGA+U to explore the electronic structure of $EuMn_2P_2$ and how it might give rise to our observations. $EuMn_2P_2$ crystallizes in a trigonal lattice (space group *P*-3m1, Tables SIV,SV,SVI and Fig. 2A), and is built of layers of Eu^{2+} cations and $(Mn_2P_2)^{2-}$ bilayers. Calculations with A-type antiferromagnetic order and a Hubbard U on the Eu atoms, in agreement with prior experiments,[17] and non-magnetic Mn atoms predict metallic behavior, in disagreement with experiment. Indeed, the Mn d-orbitals dominate the Fermi level, Fig.S10A, as expected for Mn which has a partly filled d-orbital manifold. However, introducing magnetism on Mn by either setting an antiferromagnetic Mn order without a Hubbard U or Mn ferromagnetic order with a Hubbard U also results in metallic behavior (Fig. S9). It is only when a Hubbard U and antiferromagnetic order on the Mn ions is included, along with a Hubbard U and antiferromagnetism on Eu, that semiconducting behavior is predicted, Fig. 2D,2E,2F and Fig. S10B. Inclusion of spin orbit coupling (SOC), Fig. S11, has a negligible effect on the band structure and symmetry analysis confirms that the compound is a topologically trivial insulator. These results suggest that the band narrowing associated with Mn antiferromagnetic exchange plays a pivotal role in opening a band gap and thus we classify $EuMn_2P_2$ as a Mott insulator.

In order to use these calculations to understand the appearance of non-linear IV transport, it is necessary to compare the electronic structures with and without Eu magnetic order. As the states near E_f are dominated by Mn in the $(Mn_2P_2)^{2-}$ layers, this necessitates a proper understanding of the behavior of Mn. Since these calculations require Mn antiferromagnetic order in order to produce a semiconducting ground state, and yet Mn order had not previously been reported in $EuMn_2P_2$,[17] we carried out a series of experiments to clarify whether the Mn in $EuMn_2P_2$ is magnetically ordered or not. No sign of a magnetic phase transition for Mn is found in temperature-dependent magnetization measurements from T = 2-700 K, Fig. S3, S4, S15, and Differential Scanning Calorimetry (DSC) measurements from T = 450-580 K, Fig. S16. Temperature-dependent specific heat from T = 2-250 K, Fig. 3A, also shows no evidence of a magnetic phase transition for Mn. There is a λ anomaly indicative of a magnetic ordering transition at T_N = 17 K, as expected for Eu magnetic order, but no anomalies above T = 100 K. This is in contrast to isostructural $EuMn_2X_2$ (X = Sb, As), for which antiferromagnetic Mn order is known at T_N = 120 K and T_N = 140 K respectively.[18-20] If $EuMn_2P_2$ continued the trend, one would be expected near $T_N \sim 160$ K, which is not observed. However, in addition to shifting to higher temperatures, the transition becomes broader going from X = Sb to X = As, so it is possible the Mn magnetism is still present, but manifests as a cross over or other broad change, rather than as a proper phase transition.

To check for the presence of local Mn magnetic order, we use magic angle spinning (MAS) ^{31}P NMR as a probe of the local environment, Fig. 3B. At T=295K, there is a sharp peak which is consistent with the single crystallographic site for P in the crystal structure. However, on lowering the temperature, there is a monotonic broadening of the MAS line, in addition to a Knight shift. The variation in the Knight shift tracks the bulk susceptibility (Fig. S17, S18) and suggests it arises from the magnetism on the Eu ions The line broadening is caused by the magnetic field inhomogeneity in the grains of paramagnetic powder and is proportional to the bulk magnetic susceptibility as well. There is weak evidence of the Mn

contributions in the magnetization data at lower fields, Fig.S3: Curie-Weiss analysis gives a Curie constant per formula unit of C=8.9 emu.K.mol-f.u.$^{-1}$Oe^{-1}. This is larger than the expected value for pure high spin Eu^{2+} (S=7/2), C = 7.9 emu.K.mol-f.u.$^{-1}$Oe^{-1}, suggesting a contribution of ~1 emu.K.mol-f.u.$^{-1}$Oe^{-1} from Mn. This is much less than the extra ~8 emu.K.mol-f.u.$^{-1}$Oe^{-1} that would be expected from high spin Mn^{2+}, suggesting a greatly reduced magnetic response from Mn, if present – this is consistent with the strong covalent bonds in the Mn-P framework, which are known to reduce magnetic moments.[22]

Entropy losses associated with magnetism can definitively resolve whether Mn order is present. We measured the specific heat on isostructural $EuZn_2P_2$. This compound replaces Mn with non-magnetic Zn, but otherwise keeps a very similar atomic mass, and thus serves as a suitable non-magnetic reference. We find that there is excess entropy in the case of $EuMn_2P_2$, spread over a broad range T ~ 65-250 K, Fig. 3C. By properly adjusting for the small difference in molecular mass and carrying out appropriate interpolation at low temperature, the phonon contribution to the specific heat can be estimated and removed (Fig. S19 and Table-SVII) to leave the magnetic specific heat, C_{mag}. Integration of C_{mag}/T yields the entropy change associated with magnetism, Fig. 3D. Since ^{151}Eu Mössbauer, Fig. S1, indicates all Eu is in the 2+ oxidation state ($4f^7$, S = 7/2), we expect to recover a $\Delta S_{mag} = Rln(2S+1) = Rln(8)$ per Eu ion. Indeed, there is a plateau in ΔS_{mag} just below $Rln(8)$ around T ~ 50 K, with the discrepancy attributable to the imprecision in the Eu entropy recovered below our base temperature to T = 0 K. However, there is then a gradual rise over T ~ 65-250 K to a value approximately $Rln(8) + Rln(6)$. This excess entropy cannot be from the Eu ion, as it is L = 0, there are no low-lying crystal field levels and the Eu is valence precise at 2+, and thus instead naturally attributed to magnetism on Mn. High spin Mn would be S = 5/2, so we'd expect an additional entropy recovery of $\Delta S_{mag} = 2Rln(2S+1) = 2Rln(6)$ [there are two Mn ions per Eu ion]. This is about twice what is observed, suggesting either that the Mn^{2+} is not rigorously high spin, that the Mn magnetic lattice is not fully magnetically ordered, or that a more exotic magnetic ground state (e.g. a quantum spin liquid) is present, all of which are in agreement with magnetization measurements. Future work should explore these possibilities in greater detail. Regardless, these data show that there is Mn magnetism present in $EuMn_2P_2$, resolving the discrepancy with our DFT calculations.

We thus return to DFT in order to understand the magnetic and electronic behavior of $EuMn_2P_2$. By computing the energy of different antiferromagnetic configurations, we can use DFT to predict the intermediate-temperature and low temperature magnetic configurations of this material, including both Mn and Eu magnetism. Since the SOC is negligible we consider A-type, C-type and G-type antiferromagnetic configurations for Mn. For the intermediate-temperature configuration we set the Eu f-orbitals in the core and we find that the C-type configuration, Fig. 2C,G,H is the lowest in energy. Such assignment is in agreement with the observation of a sharp magnetic phase transition when Eu orders below T=17K because of lowering in the symmetry. In contrast, the close-in-energy G-type Mn order would have resulted in a crossover instead of transition for Eu ordering, Fig. S12, as there would no longer be a change in symmetry. The C-type magnetic structure for Mn is also observed in the isostructural analog $EuMn_2As_2$.[18,19]

The corresponding band structure and density of states with Mn magnetic order and Eu in the core, Fig. 2G,H, give a small indirect band gap, ~0.45 eV. This indirect gap decreases significantly to ~0.29 eV when Eu magnetic order is considered due to exchange splitting of the conduction band states, Fig. 2E,F. In both cases, the direct gap is markedly larger, ~1.3 eV. These gaps are in agreement with room

temperature optical reflectivity measurements, Fig. S13, which shows a tail of absorption down to ~0.2 eV with a sharp edge at ~0.7 eV, and also in agreement with temperature-dependent resistivity measurements, Fig. S14.

Our observations can thus be explained as follows, Fig. 4 and S20: above the Eu magnetic ordering transition, electrical transport is driven by an impurity band lying in the band gap, with only a single set of readily accessible states, Fig. 4A. The appearance of Eu magnetic order causes a shift in the position of the conduction band edge of $EuMn_2P_2$, making it accessible (in addition to an impurity band living in the gap) for transport, when sufficiently biased by the metallic contacts, Fig. 4B. An alternative explanation also consistent with these calculations is that there is an impurity band whose position shifts upon formation of magnetic order. In either scenario, a plausible microscopic mechanism is that the Eu 4f ordering conspires with the antiferromagnetic order of the $(Mn_2P_2)^{2-}$ framework to drive large changes in states available for conduction near the chemical potential of the metallic contacts. Unfortunately, the difficulty in simulating paramagnetic states within DFT precludes exploring this in more detail computationally. We note that similar splitting of states in different sublattices due to magnetic has been observed in other compounds, such as in $MnBi_2Te_4$ and $Eu_5In_2Sb_6$.[22,23]

It is natural to ask why $EuMn_2P_2$ behaves differently from to $EuMn_2As_2$ and $EuMn_2Sb_2$. Not only does the former not show a proper Mn magnetic phase transition, but the latter are found to exhibit metallic (or very heavily doped semiconductor) conductivity. The bond distances between Mn-X (X=P, As, and Sb) increase as X's ionic radius becomes larger, Fig. 3A. Combined with an increased in the difference in electronegativity, this reduces the covalency of the $(Mn_2X_2)^{2-}$ network and results in more "ionic" behavior from the Mn cations, Table-SVIII. This explains the more definitive magnetic transitions from X = P to As and Sb. At the same time, the valence and conduction bands become broader going from X = P to X = Sb due to larger orbitals on the anions, which reduces the gap and explains the higher metallicity.

In summary, we report the discovery of the appearance of non-linear IV transport in semiconducting $EuMn_2P_2$ single crystals below T_N=17 K with the onset of Eu^{2+} magnetic order. The underlying cause appears to be a substantial exchange splitting of $(Mn_2P_2)^{2-}$ states with the occurrence of Eu order. Our observations are consistent with tunneling into defect states or an impurity band dominating the transport (cf the "excess current" contribution of the Sze model[24] and the variable range hopping analysis of Fig. S21, S22). This by itself is not uncommon, except it "turns on" at the magnetic ordering temperature (17-18 K), due to the formation of magnetic order radically adjusting the band levels in this material. This discovery opens new avenues to studying the band effects of magnetic order in, and developing useful electronic devices from, Mott insulators.

Acknowledgements
The authors acknowledge Collin L. Broholm, Mazhar Ali, Johannes Gooth, Defa Lui, Vincent Morano, Shannon Bernie, Maxime Siegler and Rauf Koban for helpful discussions.

Funding: This research was conducted at the Institute of Quantum Matter, an Energy Frontier Research Center funded by the U.S. Department of Energy Office of Science, Basic Energy Sciences, under Award No. DE-SC001933. Financial support for this work was provided by Fonds Qu'eb'eco de la Recherche sur la Nature et les Technologies, and the Natural Sciences and Engineering Research Council (NSERC)

Canada. Work in Tallinn was funded by the European Regional Development Fund (Awards TK133 and TK134) and the Estonian Research Council (Projects PRG4 and IUT23-7). This work was also financially supported by the European Research Council (ERC Advanced Grant No. 742068 'TOPMAT'). We also acknowledge funding by the DFG through SFB 1143 (project ID. 247310070) and the Würzburg-Dresden Cluster of Excellence on Complexity and Topology in Quantum Matter ct.qmat (EXC2147, project ID. 39085490)

Author contributions: T.B designed the material and experiments under the supervision of T.M.M. T.B. and V.J.S. grew single crystals under supervision of T.M.M. T.B and C.M.P. solved the single crystal structure. N.V. and D.V. carried out and interpreted the DFT calculations. D.R. designed and executed the ^{151}Eu Mössbauer measurements. . R.R., I.H. and R.S. designed and executed the NMR measurements. R.B. and N.P.A. carried out the IR reflectivity measurements. T.B. carried out the electrical transport measurements with advice from N.K. and W.S. under the supervision of C.F. The manuscript was written with input from all authors.

Competing interests: The authors declare no competing financial interests.

Data and materials availability: Experimental data files are available upon reasonable request from the corresponding author.

References

1. F. Iga, N. Shimizu, T. Takabatake, Single crystal growth and physical properties of Kondo insulator YbB_{12}, *Journal of Magnetism and Magnetic Materials,* **177**, 337–338 (1998).
2. T. Nagatsuma, G. Ducournau, C. Renaud, Advances in terahertz communications accelerated by photonics. *Nature Photon,* **10**, 371–379 (2016).
3. W. T. Fuhrman, J. Leiner, P. Nikoli´c, G. E. Granroth, M. B. Stone, M. D. Lumsden, L. DeBeer Schmitt, P. A. Alekseev, J.-M. Mignot, S. M. Koohpayeh, P. Cottingham, W. Adam Phelan, L. Schoop, T. M. McQueen, C. Broholm, Interaction driven subgap spin exciton in the kondo insulator SmB_6, *Physical Review Letters*. **114**, 036401 (2015).
4. P. Bonville, F. Rullier-Albenque, D. Colson, D., A Forget, Incommensurate spin density wave in Co-doped $BaFe_2As_2$. *Europhysics Letters*. **89**, 67008 (2010).
5. J. Gooth, B. Bradlyn, S. Honnali, C. Schnindler, N. Kumar, J. Noky, Y. Qi, C. Shekhar, Y. Sun, Z. Wang, B. A. Bernevig, C. Felser, Axionic charge-density wave in the Weyl semimetal $(TaSe_4)_2I$. *Nature*, **575**, 315–319 (2019).
6. P. J. W. Moll, P. Kushwaha, N. Nandi, B. Schmidt, A. P. Mackenzie, Evidence for hydrodynamic electron flow in $PdCoO_2$. *Science* **351**, 1061–1064 (2016).
7. V. Georgios, A. S. Jermyn, A. Polina, F. Claudia, N. Prineha, Electron hydrodynamics in anisotropic materials. *Nature Communication*, **11**, 4710 (2020).
8. A. Devarakonda, H. Inoue, S. Fang, C. Ozsoy-Keskinbora, T. Suzuki, M. Kriener, L. Fu, E. Kaxiras, D. Bell, J. Checkelsky, Clean 2D superconductivity in a bulk van der Waals superlattice, *Science*, **370**, 231 (2020).
9. B. R. Ortiz, P. M. Sarte, E. M. Kenney, M. J. Graf, S. M. L. Teicher, R. Seshadri, S. D. Wilson, Superconductivity in the *Z*2 kagome metal KV_3Sb_5, *Physical Review Materials*, **5**, 034801 (2021).

10. T. Berry, S.R. Parkin, T.M. McQueen, Antiferro- and Meta-magnetism in the *S*=7/2 Hollandite Analog $EuGa_2Sb_2$, *Physical Review Materials*, **5**, 114401 (2021).
11. M. Sinha, H.K. Vivanco, C. Wan, M.A. Siegler, V.J. Stewart, L.A. Pressley, T. Berry, Z. Wang, I. Johnson, M. Chen, T.T. Tran, W.A. Phelan, T.M. McQueen, Twisting of 2D Kagome Sheets in Layered Intermetallics, *ACS Central Science*, **7**, 1381-90 (2021).
12. Y. Yu, L. Ma, P. Cai, R. Zhong, C. Ye, J. Shen, G. D. Gu, X. H. Chen, Y. Zhang, High-temperature superconductivity in monolayer $Bi_2Sr_2CaCu_2O_{8+\delta}$, *Nature,* **575**, 156–163 (2019).
13. I. Guillamón, H. Suderow, S. Vieira, L. Cario, P. Diener, P. Rodière, Superconducting density of states and vortex cores of 2H-NbS_2, *Physical Review Letters*, **101**, 166407 (2008).
14. A. Alexandradinata, C. Wang, W. Duan, L. Glazman, Revealing the topology of Fermi-surface wave functions from magnetic quantum oscillations. *Physical Review X*, **8**, 011027 (2018).
15. S. Gundogdu, J. P. Clancy, G. Xu, Y. Zhao, P. A. Dube, T. C. Karalar, B. Ki Cho, J. W. Lynn, M. Ramazanoglu, Magnetic order and competition with superconductivity in (Ho-Er)Ni_2B_2C, *Materials Research Express*, **7**, 11, 116002 (2020).
16. H. S. Jeevan, Z. Hossain, D. Kasinathan, H. Rosner, C. Geibel, P. Gegenwart, High-temperature superconductivity in $Eu_{0.5}K_{0.5}Fe_2As_2$, *Physical Review B*, **78**, 092406 (2008).
17. A. C. Payne, A. E. Sprauve, M. M. Olmstead, S. M. Kauzlarich, J. Y. Chan, B. A. Reisner, J. W. Lynn, Synthesis, magnetic and electronic properties of single crystals of $EuMn_2P_2$. *Journal of Solid State Chemistry*, **163**, Issue 2 (2002).
18. V. K. Anand and D. C. Johnston, Metallic behavior induced by potassium doping of the trigonal antiferromagnetic insulator $EuMn_2As_2$, *Physical Review B*, **94**, 014431 (2016).
19. A. Dahal, Y. Chen, T. Heitmann, A. Thamizhavel, U. Paramanik, S. K. Dhar, D. K. Singh, Spin correlation in trigonal $EuMn_2As_2$, *Physical Review B*, **99**, 085135 (2019).
20. I. Schellenberg, M. Eul, W. Hermes, R. Pöttgen, A ^{121}Sb and ^{151}Eu Mössbauer Spectroscopic Investigation of $EuMn_2Sb_2$, $EuZn_2Sb_2$, $YbMn_2Sb_2$, and $YbZn_2Sb_2$, *Zeitschrift für anorganische und allgemeine Chemie*, **636**, 85 (2010).
21. M. Roberg, T. Reveyrand, I. Ramos, E. A. Falkenstein, Z. Popovic, High Efficiency Harmonically Terminated Diode and Transistor Rectifiers, *IEEE Trans. Microwave Theory Technology*, **60**, 4043–4052 (2012).
22. D. Zhang, M. Shi, T. Zhu, D. Xing, H. Zhang, J. Wang, Topological axion states in the magnetic insulator $MnBi_2Te_4$ with the quantized magnetoelectric effect. *Physical Review Letters,* **122**, 206401 (2019).
23. P. Rosa, Y. Xu, M. Rahn, J. Souza, S. Kushwaha, L. Veiga, A. Bombardi, S. Thomas, M. Janoschek, E. Bauer, M. Chan, Z. Wang, J. Thompson, N. Harrison, P. Pagliuso, A. Bernevig, F. Ronning, Colossal magnetoresistance in a nonsymmorphic antiferromagnetic insulator. *npj Quantum Materials*, **5**, 52 (2020).
24. M. Veldhorst, M. Snelder, M. Hoek, C. G. Molenaar, D. P. Leusink, A. A. Golubov, H. Hilgenkamp, A. Brinkman, Magnetotransport and induced superconductivity in Bi based three‐dimensional topological insulators, *Physica Status Solidi RRL*, **7**, 26 (2013).

Fig. 1. The onset of nonlinear voltage current behavior below the Eu magnetic ordering temperature of T_N=17K in $EuMn_2P_2$ single crystals as seen in **(a)** T=20K, **(b)** T=15, **(c)** T=5K, and **(d)** T=2K. **(e)** The magnetic field dependence of voltage current behavior with $\mu_oH\perp$c at T=2K showing the non-linear behavior is only slightly affected by an applied magnetic field. **(f)** The correlation between the hyperfine field from Mössbauer spectroscopy with the fraction diode current model at μ_oH=0T and μ_oH=9T, showing the "turn on" of non-linear behavior with the appearance of antiferromagnetic order on Eu. **(g)** The resistance, dV/dI, as a function of potential difference at μ_oH=0T and μ_oH//c. The blue frame is the region where $V\rightarrow 0$ pertaining to the conduction channel associated to the non-linearity in the voltage-current plots. **(h)** The temperature dependence of the resistance associated as $V\rightarrow 0$ from the blue region in (g) at μ_oH=0T and μ_oH//c. **(i)** The normalized resistivity in (h), but plotted vs. $\frac{1}{T^{1/2}}$. A $T^{1/2}$ scaling is suggestive of 1-dimensional variable-range-hopping in the $V\rightarrow 0$ from the blue region in (g) at μ_oH=0T and μ_oH//c.

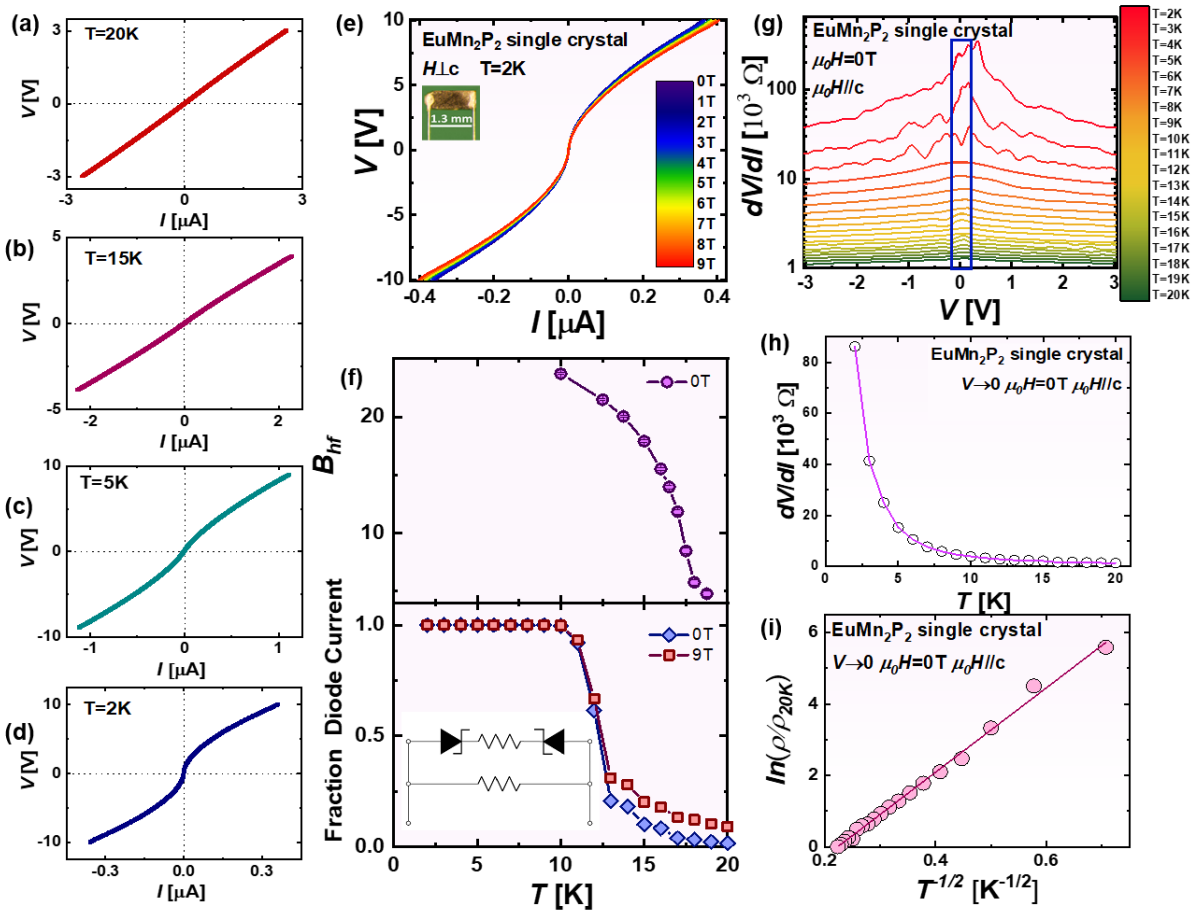

Fig. 2. **(a)** $EuMn_2P_2$ is a non-symmorphic crystal structure that crystallizes in space group *P*-3m1, No. 164. The crystal structure consists of anionic framework on $(Mn_2P_2)^{2-}$ with tetrahedral framework and Eu^{2+} cations occupying the corner sites. **(b)** A picture of grown single crystal of $EuMn_2P_2$. **(c)** Predicted intermediate-temperature magnetic structure with C-type antiferromagnetic order of Mn. **(d)** Predicted low-temperature magnetic structure with the same Mn ordering and A-type antiferromagnetic order of Eu and enlargement of the unit cell. **(e)** The electronic band structure and density of states within GGA+U following the magnetic structure as shown in (d). As expected from the bonding framework, the states near the Fermi level (E_f) are coming from Mn-d states, where as the Eu-f states are further away from the E_f. **(f)** The density of states (DOS) associated to the band structure in (e). **(g)** The electronic band structure and density of states within GGA+U following the magnetic structure as shown in (c). **(h)** The DOS associated to the band structure in (f).

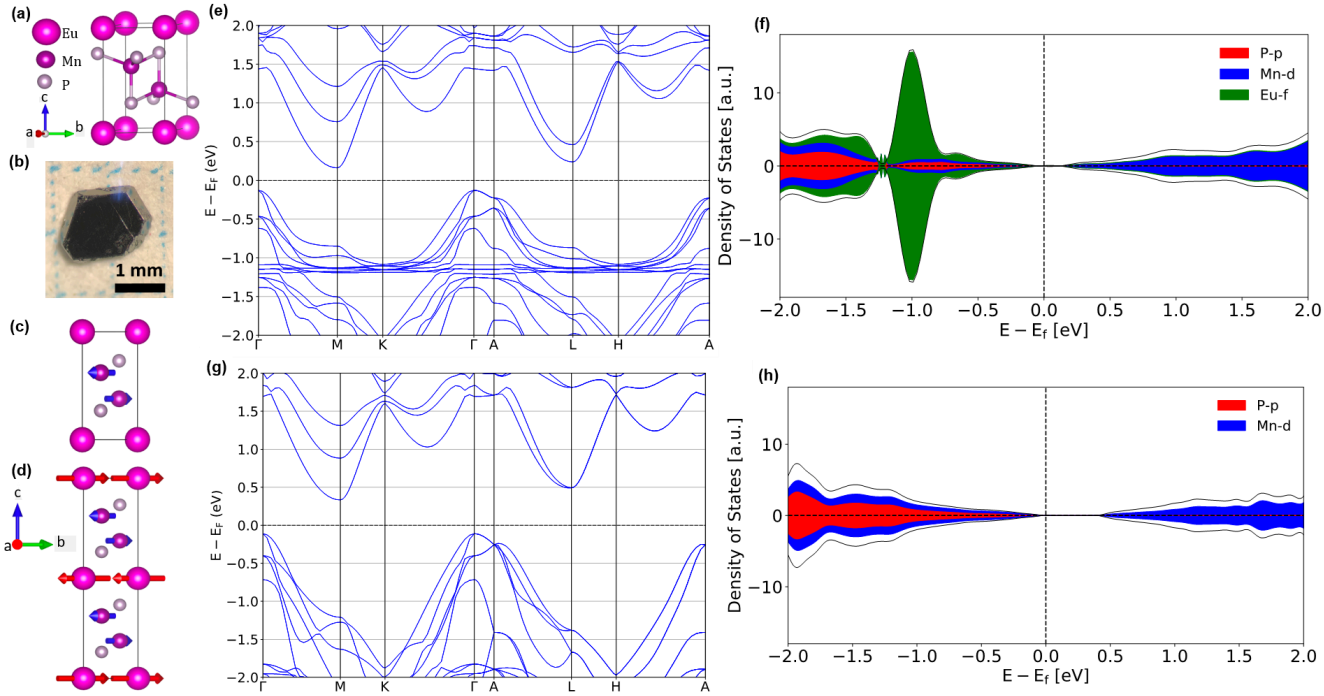

Fig. 3. **(a)** Heat capacity as a function of temperature for $EuMn_2P_2$, $EuMn_2As_2$, and $EuMn_2Sb_2$ single crystals.[20,23] The phase transition close to T=20K is attributed to Eu magnetic order, while the transition close to T=130K is attributed to Mn order. Note, that the transition becomes weaker as we go from Sb to As, and transition seems absent in P in the $EuMn_2X_2$ structure. The Mn phase transition in Mn has a direct relation on the bond distances between Mn-P and Mn to neighboring Mn within the structure. **(b)** $EuMn_2P_2$ temperature dependence of ^{31}P NMR spectrum. The line shift, as well as the line broadening both follow the magnetic susceptibility. **(c)** Temperature-dependent heat capacity of $EuMn_2P_2$ and $EuZn_2P_2$ single crystals at $\mu_o H$ = 0.1 T from T = 2–300 K. The sharp transition at T_N =17 K in $EuMn_2P_2$ and T_N =21K in $EuZn_2P_2$ are attributed to the antiferromagnetic phase transitions. The inset shows the magnified antiferromagnetic phase transitions at T_N=17 K and T_N =21K. **(d)** The change in magnetic entropy was integrated after subtracting the phonons from T=2–300 K. The ΔS_{mag} is close to the Rln(8) expected for an L = S = 7/2 system at T=17K, with an additional contribution from Mn at higher temperatures.

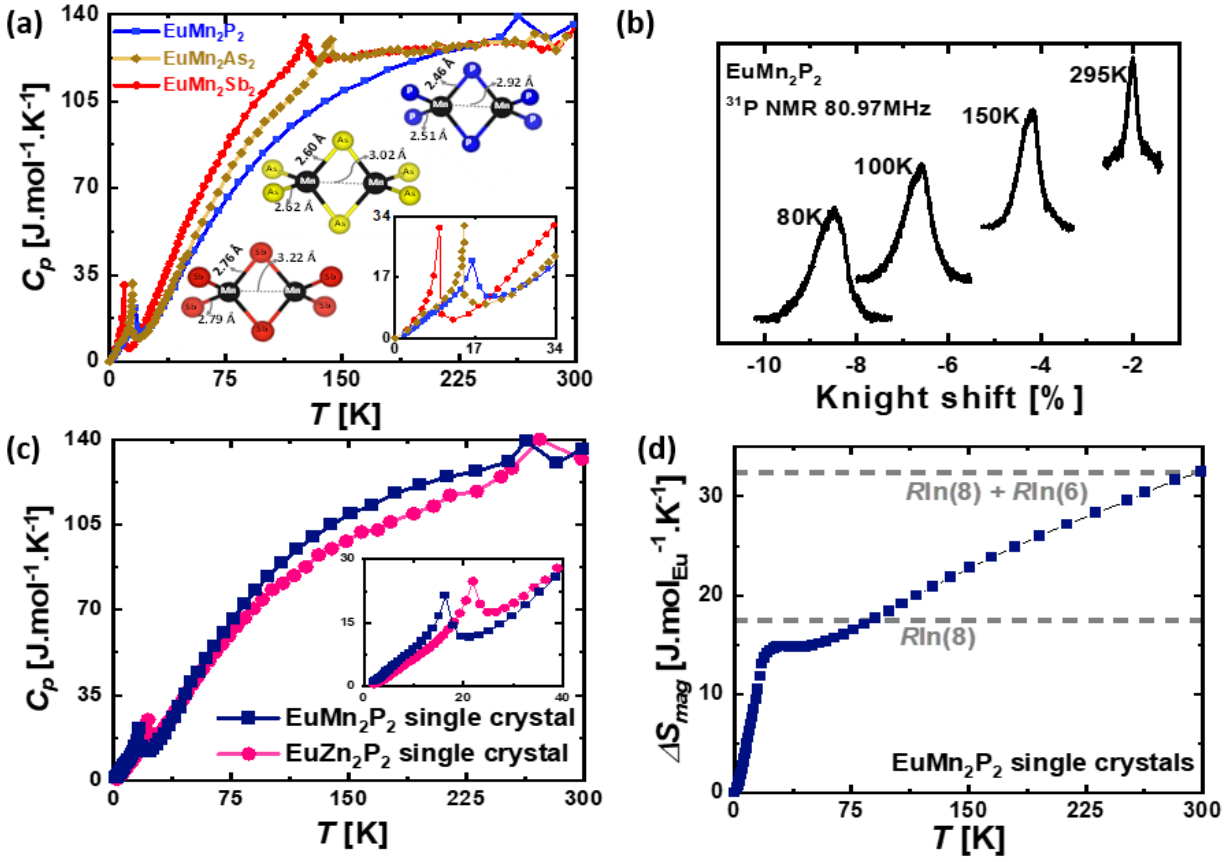

Fig. 4. The mechanism of the switch on of non-linear voltage-current behavior in the single crystals of $EuMn_2P_2$ with the onset of Eu magnetic order at T_N=17K. **(a)** Above T_N, the IV curve is linear, and the indirect gap is 0.445 eV. Conduction is thus dominated by an impurity band located somewhere in the gap, shaded orange. **(b)** When the Eu atoms magnetically order, there is a large exchange splitting of the $(Mn_2P_2)^{2-}$ derived conduction band states. This reduces the indirect gap to 0.29 eV, and makes accessible a second set of states (from the conduction band), when an appropriate voltage is applied to the metallic contacts. This gives rises to impurity-band-driven transport at low voltages, and impurity-and-conduction band driven transport at high voltages.